PROCEEDINGS OF SCIENCE

ONLINE ICRC 2021
THE ASTROPARTICLE PHYSICS CONFERENCE
Berlin | Germany
37th International Cosmic Ray Conference
12–23 July 2021

The Advanced Particle-astrophysics Telescope: Simulation of the Instrument Performance for Gamma-Ray Detection

Wenlei Chen[a,*] **and James H. Buckley**[b] **on behalf of the APT Collaboration**
(a complete list of authors can be found at the end of the proceedings)

[a] *University of Minnesota, Twin Cities*
School of Physics and Astronomy, 116 Church Street SE, Minneapolis, MN 55455, USA
[a] *Washington University in St. Louis,*
Dept. Physics, One Brookings Drive, Saint Louis, MO, USA
E-mail: chen6339@umn.edu, ...

We present simulations of the instrument performance of the Advanced Particle-astrophysics Telescope (APT), a mission concept of a γ-ray and cosmic-ray observatory in a sun-Earth Lagrange orbit. The key components of the APT detector include a multiple-layer tracker composed of scintillating fibers and an imaging calorimeter composed of thin layers of CsI:Na scintillators. The design is aimed at maximizing effective area and field of view for γ-ray and cosmic-ray measurements, subject to constraints on instrument cost and total payload mass. We simulate a detector design based on 3-meter scintillating fibers and develop reconstruction algorithms for γ-rays from a few hundreds of keV up to a few TeV energies. At the photon energy above 30 MeV, pair-production/shower reconstruction is applied; the results show that APT could provide an order of magnitude improvement in effective area and sensitivity for γ-ray detection compared with the Fermi Large Area Telescope (LAT). A multiple-Compton-scattering reconstruction at photon energies below 10 MeV achieves sensitive detection of faint γ-ray bursts (GRBs) and other γ-ray transients down to ~ 0.01 MeV/cm^2 with degree-level to sub-degree-level localization accuracy. The Compton analysis also provides a measurement of polarization where the minimum detectable degree of polarization for $\sim$ 1 MeV/cm^2 GRBs is below 20%. In addition to the APT simulations, we present the simulated performance of the Antarctic Demonstrator for APT, a 0.5m-square cross section balloon experiment that includes all of the key elements of the full APT detector.

37th International Cosmic Ray Conference (ICRC 2021)
July 12th – 23rd, 2021
Online – Berlin, Germany

*Presenter

PoS(ICRC2021)590

1. The Advanced Particle-astrophysics Telescope and the Antarctic Demonstrator

The Advanced Particle-astrophysics Telescope (APT) is a high-energy γ-ray and cosmic-ray mission concept. The instrument design is aimed at maximizing effective area and field of view for MeV-TeV gamma-ray and cosmic-ray measurements. Considering the limits to the payload mass and instrument cost, we propose a detector design based on 3-meter scintillating fibers read out by Silicon photomultipliers (SiPMs). The APT detector includes a multiple-layer tracker composed of scintillating fibers and an imaging calorimeter composed of thin layers of sodium-doped CsI (CsI:Na) scintillators and wavelength-shifting (WLS) fibers. The CsI:Na crystals are coupled to crossed planes of wavelength shifting fibers to localize energy deposition to ~mm accuracy. With about half of the number of electronic readout channels of the Fermi Gamma-ray Space Telescope (FGST) Large Area Detector (LAT) and a relatively shallow (< 6 radiation length) calorimeter, our simulations show that the critical performance requirements can be met within a reasonable payload mass for available launch vehicles. The Antarctic Demonstrator for APT (ADAPT) is a balloon experiment with a 1/2 meter square aperture, and 4 fully instrumented tracker/imaging-CsI-calorimeter (ICC) layers The ADAPT experiment will demonstrate the potential of our instrument concept and test our γ-ray and cosmic-ray reconstruction algorithms as well as providing some measurements of GRBs that occur during the long-duration balloon flight. The major scientific goals of the APT experiment include fast, all-sky, and large effective area detection and localization of γ-ray bursts (GRBs) and other γ-ray transients such as gravitational wave counterparts (e.g., [1]). Another key objective is to conduct a search for thermal dark-matter particles over the entire natural range of masses and total annihilation cross section. A more detailed description of the APT and ADAPT science goals, instrument design, and project status can be found in [2].

In this paper, we present simulations of the instrument performance of the APT for incident γ-rays with energies from 0.3 MeV to 1 TeV. The detector simulation is calibrated by laboratory measurements of prototype scintillating fiber and CsI detectors. Multiple-Compton-scattering reconstruction is used in the low-energy range (< 30 MeV) and pair-production reconstruction is applied at the photon energy $\geq$ 30 MeV. The simulated instrument performance shows significant improvements not only in effective area and geometry factor, but also in position localization for MeV transients, increased sensitivity for low energy pair events, and sensitivity and angular resolution for high energy (~100) GeV astrophysical sources.

2. Detector Construction

The baseline APT detector has a uniform, multi-layer structure. Each layer of the detector consists of an array of cylindrical, multi-clad scintillating fibers that serve as a tracker (there is both an x and y-fiber plane in each layer, each composed of two interleaved layers of close-packed fibers), supporting materials (possibly serving as a transition-radiation radiator), a thin CsI:Na crystal layer coupled to a top (x) and bottom (y) plane of 2 mm square WLS fiber that behaves as both a pair-converter and a calorimeter. The baseline instrument has a 3 m $\times$ 3 m active area with $20-40$ detector layers, limited by the size of the fairings (and lift capacity) of existing launch vehicles. The instrument is symmetric with respect to upward or downward going particles, doubling the effective field of view for a high (e.g., Lagrange point) orbit. Additionally, the use of a fully active detector

volume consisting of CsI crystals and scintillating fibers and a relatively modest calorimeter depth ($\sim$ 5.8 radiation lengths, for 20 detector layers with 5 mm-CsI crystals including mechanical support structure) in place of the passive tungsten trackers, silicon strips, and CsI crystal blocks used in the Fermi-LAT (with $\gtrsim$ 10 radiation lengths of depth) would make it possible to achieve the required performance goals while limiting the weight of the instrument. Figure 1 shows the geometry of the APT main detector. A single 3 m $\times$ 3 m 20-layer instrument of 5.8 radiation lengths would weigh approximately 7,200 kg. The recent success of the SpaceX Falcon-heavy rocket increases our confidence that the total instrument weight should not exceed the lift capacity to a high (Lagrange) orbit.

The current design of the ADAPT includes four layers of scintillating-fiber-tracker and ICC modules of 45 mm $\times$ 45 mm. We will also place photo detectors on the edges of the CsI:Na crystal to collect the totally-internally reflected scintillation light that is not transmitted into the WLS fibers (a potential modification of the APT design under consideration). On the bottom of the 4-layer imaging detector, there will be 4 additional layers of CsI:Na calorimeter without wavelength-shifting fibers to increase the radiation length of the detector for GeV γ-ray observations.

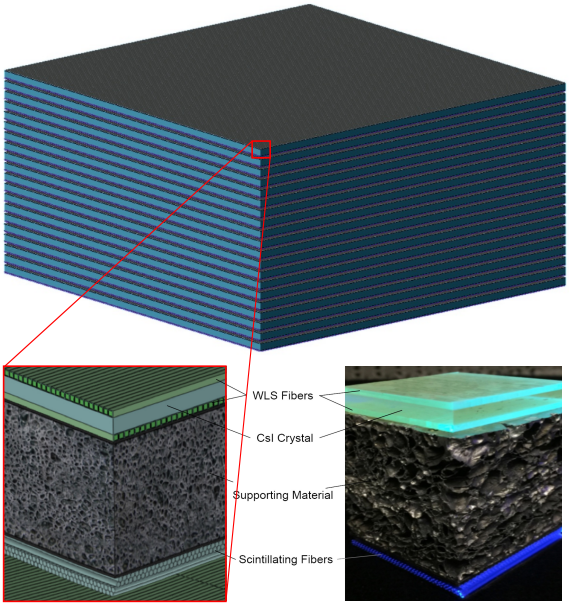

Figure 1: Top: the APT main detector. Bottom: one layer of the APT detector prototype. (Left: solid model of the detector geometry. Right: a small cross section constructed out of actual scintillating fibers and an aluminum honeycomb for demonstration.)

3. APT Instrument Simulation and Event Reconstruction

To validate and optimize our detector approach for electromagnetic-shower tracking and multiple-Compton reconstruction, we developed a software package (APTsoft[1]) including scripts to generate geometry/configuration files, Geant4[3] code to simulate γ-ray and cosmic-ray interactions with the detector, optical simulation code of light collection and electronics detection, and γ- and cosmic-ray analysis tools to calculate instrument performance. The simulated APT geometry with a normal-incident 1 GeV γ-ray is shown in Figure 2, where the optical signals are collected on the sides of the detector, as illustrated. The specifications of the detector response for the simulations are derived from measured performance parameters from prototype tracker fibers and a prototype of the CsI detector. We include a simple detector simulation where we assume the SiPM signals are registered by waveform digitizers with similar parameters to the Target C ASICs used in our prototype instruments.

[1]The software is available from the corresponding authors upon reasonable request.

The instrument performance is calculated by statistically evaluating the difference between the simulated γ-ray event parameters with the reconstructed event parameters. At energies above $\sim$ 30 MeV, pair production is the dominant photon interaction in the detector material. At lower energies ($\lesssim$ 10 MeV), incident γ-rays experience multiple Compton scatterings until depositing their total energy in the detector (or escaping). The APT instrument will function both as a pair telescope for 30 MeV to $\sim$ 1 TeV γ-rays and as a Compton telescope with excellent sensitivity down to $\sim$ 0.3 MeV. The Compton- and pair-events are reconstructed differently with an energy gap at $\sim 10 - 30$ MeV, where event acceptances of the instrument in these two detection modes vanish and the pair- and Compton-events can not be easily distinguished.

We developed a simple trajectory/shower-fitting algorithm for the pair-event reconstruction. For energy reconstruction of pair events, the energy deposition of an incident γ-ray in the CsI crystal can be described by a function of the propagation distance in units of radiation length (X_0). The normalized profile of the expected energy deposition for a γ-ray event at energy E is given by

$$f(x, E) = \frac{1}{2\Gamma(\epsilon)} \left(\frac{\hat{x}}{2}\right)^{\epsilon-1} e^{-\hat{x}/2}, \qquad (1)$$

where $\Gamma(x)$ is the gamma function, $\epsilon = 2 + s + \ln(E)/2$, and $\hat{x} = x/X_0$. Even if the detector only captures a small fraction of the incident energy, the algorithm based on the fitting of the particle shower can still reconstruct the incident energy up to $\sim$ 1 TeV.

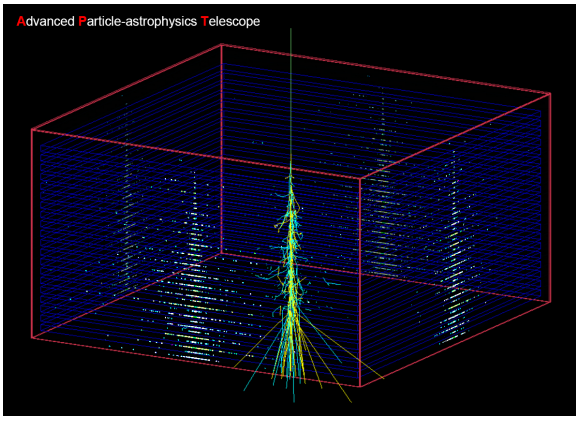

Figure 2: Simulated geometry of the APT main detector (3 m × 3 m × 1.6 m) for the simulation. Simulated particle shower and optical signals (as shown on sidewalls of the detector) for a normal-incident γ-ray event at 1 GeV is shown.

In the lower-energy Compton regime, an incident γ-ray may experience multiple Compton scatterings until its energy is fully deposited in the detector. For a sequence of k signal groups located at $P_1, P_2, ..., P_k$ with energy deposition $E_1, E_2, ..., E_k$, we find that the reconstructed angle θ_i for the i-th Compton scattering is given by

$$\theta_i = \arccos\left[1 - \left(\frac{E_e}{\sum_{j=i}^{k} E_j}\right)\left(\frac{E_i}{\sum_{j=i+1}^{k} E_j}\right)\right]. \qquad (2)$$

Clearly, θ_1 is the position angle of the incident γ-ray (the angle of the first Compton scatter), which is used to reconstruct the source position. The detector cannot distinguish the real sequence of the multiple Compton scatterings, thus $k!$ possible sequences must be given for k signal groups. Fortunately, most of the resulting θ_i values from those possible sequences are not self-consistent, i.e., $\exists i \in \{2, 3, ...k - 1\}$ that $\angle P_{i-1}P_iP_{i+1} \neq \theta_i$. As a result, we only have a few valid solutions for each event. Moreover, the solutions that do not correspond to the true incident γ-ray event are randomly distributed throughout the reconstructed sky, serving as a uniform background. The reconstructed energy of a Compton event is derived by integrating the waveforms from the ICC

detector WLS fibers (and edge detectors) and then summing over all signal groups The uncertainty of the energy reconstruction is assumed to be dominated by Poisson processes during the generation and transport of the optical photons.

For polarized incident γ-rays, the distribution of the Compton-scattering secondary γ-rays can be described by the Klein-Nishina differential cross-section formula. In the case of a linearly polarized γ-rays, the probability for the photon to be scattered at a polar angle θ and an azimuthal angle ϕ to the polarization vector is given by

$$\frac{\mathrm{d}\sigma}{\mathrm{d}\Omega} = \frac{1}{2} r_0^2 \epsilon^2 \left(\epsilon + \epsilon^{-1} - \sin^2\theta \cos^2\phi \right), \tag{3}$$

where r_0 is the classical electron radius and ϵ is the ratio between the scattered and incident γ-ray energies. Polarization of GRBs can be measured from the anisotropy of the scattered γ-rays in the APT detector.

4. Performance

4.1 Geometry factor and effective area

Figure 3 shows the acceptance (or geometry factor) of the omnidirectional-incident γ-ray events and the effective area of the normal-incident γ-ray events as functions of the incident γ-ray energy (solid black curves). Compared to the *Fermi* performance (shown in Figure 3 with dashed red curves) [4], APT provides more than an order of magnitude larger effective area and acceptance than Fermi-LAT. Moreover, the effective area of the APT instrument reaches several m^2 in the MeV regime, which is orders-of-magnitude larger than the previous experiments. COMPTEL, e.g., had an effective area of $\sim 10 - 50\ \mathrm{cm}^2$ [5]. We also include the normal-incident effective area distribution for an AMEGO-like instrument [6] in Figure 3. ADAPT's effective area and geometric factor are about two orders of magnitude smaller than the APT, consistent with its size compared to the full detector. However, the effective area of the ADAPT is comparable with the Fermi-GBM detectors in the MeV regime and exceeds that of the LAT in the $\lesssim$30 MeV pair regime.

4.2 Angular and energy resolution

The left panel in Figure 4 shows the 68% containment angle for the PSF as a function of energy (note that the angular deviation for a Compton reconstruction is defined as the shortest angular distance between the Compton ring and the real event location). As we can see, APT achieves a comparable angular resolution to *Fermi* Pass 8 SOURCE events. The right panel in Figure 4 shows the 68% containment of the fractional energy deviation $\Delta E/E$ as a function of the incident γ-ray energy. The APT energy reconstruction provides $< 20\%$ uncertainty (a standard deviation, assuming a normally distributed reconstruction error) for nearly the whole detecting energy range, where the performance is better than 10% in the $\sim 1 - 4$ MeV and $\sim 0.1 - 1$ GeV energy ranges (as shown in Figure 4). To limit payload mass, the APT calorimeter is relatively shallow with 5.4 radiation lengths of active CsI ($\sim$ 5.8 radiation lengths including fibers and support structure) along the normal direction, which is much smaller than *Fermi*'s $\sim$ 10 radiation lengths. Although the APT energy resolution is worse than *Fermi*'s at $>$ 1 GeV energies, by fitting to the longitudinal profile of showers detected by APT's imaging calorimeter, the instrument still provides acceptable measurements up to TeV energies.

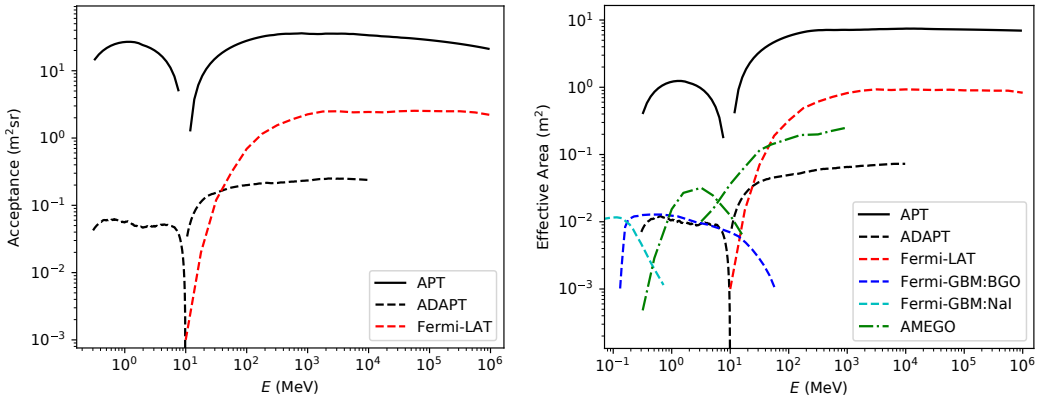

Figure 3: Acceptance/geometry factor (left) and normal-incident effective area (right) versus energy. The lower energy solid black curves denote APT Compton reconstruction and the higher denote APT pair reconstruction. Dashed red and dash-dotted green curves are for *Fermi* P8R2_SOURCE_V6 events and AMEGO, respectively. Dashed blue and cyan curves show the Fermi-GBM effective area for the BGO and NaI detectors, respectively.

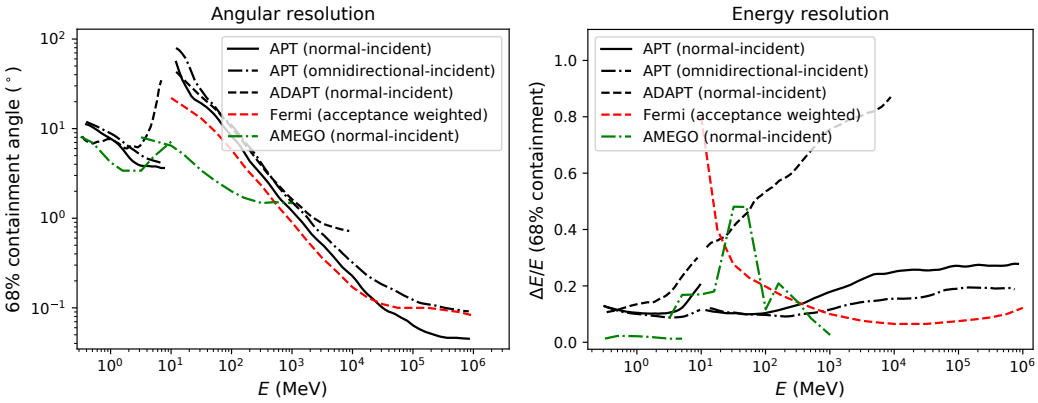

Figure 4: Angular resolution (left) and energy resolution (right) as shown by the 68% containment versus energy. Solid and dash-dotted black curves are for APT with normal- and omnidirectional-incident events. Dashed black, red, and dash-dotted green curves are for ADAPT, *Fermi* P8R2_SOURCE_V6 events, and AMEGO, respectively.

4.3 Gamma-ray burst localization and polarization

Each Compton reconstruction results in a measure of the polar Compton angle, but no determination of the azimuthal angle of the scatter, resulting in a ring-shaped uncertainty region on the sky. A transient event (e.g., GRB) can be localized by finding the centroid of the brightest region resulting from the pile-up of Compton rings in the sky map. We simulated a large number of GRBs with spectral energy distribution described by a typical Band function [7], a range of fluence values and a distribution off incident directions with inclination angles $> 45°$ from the detector's X-Y plane. For each fluence value, we simulate a number of GRBs and calculate the offset of the reconstructed position from the true source direction. The 68% containment of the offset angle is plotted as a function of fluence, as shown in Figure 5. The estimated fluence of GRB170817A

(an electromagnetic counterpart of the gravitational-wave event GW170817 [1]) in the APT energy range is shown as the red dashed line in Figure 5. As we can see, APT has degree-level accuracy of localizing faint GRBs. For bright GRBs with fluence $> 1\text{MeV/cm}^{-2}$, the APT and ADAPT have localization accuracy at sub-degree and degree levels. The right panel in Figure 5 shows an example sky map of Compton rings for a $1\ \text{MeV/cm}^{-2}$ GRB detected by the ADAPT.

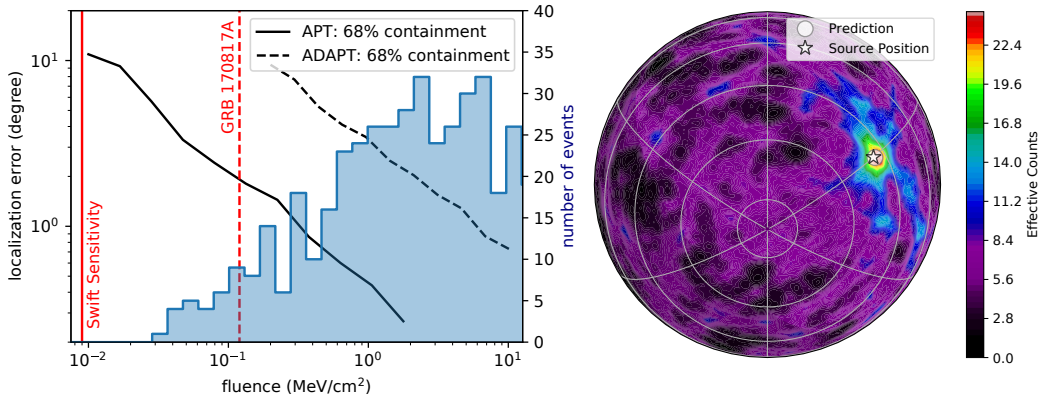

Figure 5: Left: Error in reconstructed direction of a Band-spectrum GRB versus fluence. The red solid and dashed line shows the estimated fluence of *Swift* sensitivity limit and GRB170817A/GW170817 event in the APT energy range. Histogram shows the count rate of GRBs from the first Fermi-GBM catalog [8] in the energy range from 10 keV to 1 MeV. Right: An example Compton sky map of a $1\ \text{MeV/cm}^{-2}$ GRB detected by the ADAPT.

Our simulation team also developed an independent Compton reconstruction algorithm that can provide fast, real-time event localization using a low-power flight computer. For a typical bright GRB with fluence of $1\ \text{MeV/cm}^2$, the fast algorithm can localize the event within 180ms on a single Raspberry Pi system with an localization error of $\sim 0.5°$, comparable to the result from APTsoft. A detailed description of this work can be found in [9].

Measurement of the MeV γ-ray polarization is important to understand the geometry of emission, magnetic fields and electromagnetic processes in the collimated jets of GRBs. The large effective area enables the APT detector as a very powerful Compton polarimeter to measure the γ-ray polarization from GRBs at MeV energies. We estimate the significance of the polarization measurement by evaluating the significance of getting a maximum counts value at a position angle perpendicular to the polarization vector where the count rate is minimized. For a 3-σ detecting significance, Figure 6 shows the degree-of-polarization (DOP) sensitivity for a GRB with a power-law spectrum as a function of the GRB fluence. As we can

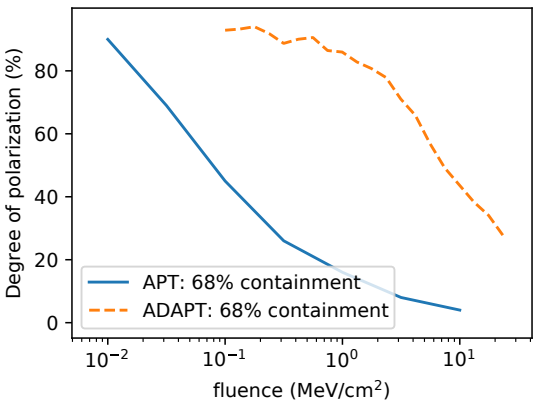

Figure 6: 3-σ DOP sensitivity of the APT and ADAPT as a function of the GRB fluence.

see in Figure 6, polarization of typical long GRBs with fluence $\gtrsim 1$ MeV/cm^2 can be significantly detected by the APT with DOP down to $\lesssim 10\%$. While for a GRB as faint as the GW170817A counterpart, the polarization can still be measurable if the γ-ray beam is highly polarized (DOP $\sim 40\%$).

5. Summary

Using multiple layers of a scintillating fiber tracker and a distributed ICC with a total thickness of $\lesssim 6$ radiation lengths, APT trades energy resolution for a very large detecting area and nearly instantaneous all-sky coverage. The imaging calorimeter allows the instrument to function both a pair telescope and a Compton telescope with excellent sensitivity from energies of 0.3 MeV up to 1 TeV. The effective area of the APT instrument reaches several m^2, which is much larger than previous experiments. Although the angular and energy resolution in the Compton regime would be somewhat limited, its large effective area and high detection efficiency would improve the MeV γ-ray sensitivity by orders of magnitude. This would result in a dramatic improvement in the localization of short γ-ray bursts compared to any extant instrument.

References

[1] B.P. Abbott, R. Abbott, T.D. Abbott, F. Acernese, K. Ackley, C. Adams et al., *Multi-messenger observations of a binary neutron star merger*, *The Astrophysical Journal* **848** (2017) L12.

[2] J. Buckley, *The Advanced Particle-astrophysics Telescope (APT) Project Status*, in *Proceedings of 37th International Cosmic Ray Conference — PoS(ICRC2021)*, vol. 395, p. 655, 2021, DOI.

[3] S. Agostinelli, J. Allison, K. Amako, J. Apostolakis, H. Araujo, P. Arce et al., *Geant4—a simulation toolkit*, *Nuclear Instruments and Methods in Physics Research Section A: Accelerators, Spectrometers, Detectors and Associated Equipment* **506** (2003) 250.

[4] https://www.slac.stanford.edu/exp/glast/groups/canda/lat_Performance.htm.

[5] V. Schoenfelder, H. Aarts, K. Bennett, H. de Boer, J. Clear, W. Collmar et al., *Instrument Description and Performance of the Imaging Gamma-Ray Telescope COMPTEL aboard the Compton Gamma-Ray Observatory*, *The Astrophysical Journal Supplement Series* **86** (1993) 657.

[6] R. Caputo, F. Kislat, J. Racusin and O.B.O.T.A. Team, *AMEGO: Simulations of the Instrument performance*, *PoS* **ICRC2017** (2018) 783.

[7] D. Band, J. Matteson, L. Ford, B. Schaefer, D. Palmer, B. Teegarden et al., *BATSE Observations of Gamma-Ray Burst Spectra. I. Spectral Diversity*, *Astrophys. J.* **413** (1993) 281.

[8] W.S. Paciesas, C.A. Meegan, A. von Kienlin, P.N. Bhat, E. Bissaldi, M.S. Briggs et al., *The fermi gbm gamma-ray burst catalog: The first two years*, *The Astrophysical Journal Supplement Series* **199** (2012) 18.

[9] M. Sudvarg, J. Buhler, J. Buckley, W. Chen, Z. Hughes, E. Ramey et al., *A Fast GRB Source Localization Pipeline for the Advanced Particle-astrophysics Telescope*, in *Proceedings of 37th International Cosmic Ray Conference — PoS(ICRC2021)*, vol. 395, p. 588, 2021, DOI.

Full Authors List: APT Collaboration

S. Alnussirat[1], C. Altomare[2], R. G. Bose[3], D. Braun[3], J. H. Buckley[3], J. D. Buhler[4], E. Burns[1], R. D. Chamberlain[4], W. Chen[5], M. L. Cherry[1], L. Di Venere[6,2], J. Dumonthier[7], M. Errando[3], S. Funk[8], F. Giordano[6,2], J. Hoffman[3], Z. Hughes[3], D. J. Huth[3], P. L. Kelly[5], J. F. Krizmanic[9,10,11], M. Kuwahara[12], F. Licciulli[2], G. Liu[13], M. N. Mazziotta [2], J. G. Mitchell[14,15], J. W. Mitchell[9], G. A. de Nolfo[15], R. Paoletti[16], R. Pillera[17,2], B. F. Rauch[3], D. Serini[2], G. Simburger[3], M. Sudvarg[4], G. Suarez[7], T. Tatoli[15,18], G. S. Varner[12], E. Wulf[19], A. Zink[8], W. V. Zober[3]

[1]Department of Physics and Astronomy, Louisiana State University, Baton Rouge, Louisiana 70803, USA, [2]Istituto Nazionale di Fisica Nucleare, Sezione di Bari, I-70126 Bari, Italy, [3]Department of Physics and McDonnell Center for the Space Sciences, Washington University, St. Louis, MO 63130, USA, [4]Department of Computer Science & Engineering, Washington University, St. Louis, MO 63130, USA, [5]Department of Physics and Astronomy, University of Minnesota, Minneapolis, MN 55455, USA, [6]Dipartimento di Fisica "M. Merlin" dell'Università e del Politecnico di Bari, I-70126 Bari, Italy, [7]NASA Goddard Space Flight Center, Greenbelt, MD 20771, USA, [8]Friedrich-Alexander-Universität Erlangen-Nürnberg, Erlangen Centre for Astroparticle Physics, D-91058 Erlangen, Germany, [9]Center for Space Sciences and Technology, University of Maryland Baltimore County, Baltimore, MD 21250, USA, [10]Astroparticle Physics Laboratory, NASA/GSFC, Greenbelt, MD 20771, USA, [11]Center for Research and Exploration in Space Sciences and Technology, NASA/GSFC, Greenbelt, MD 20771, USA, [12]Department of Engineering, University of Hawai'i at Mānoa, Honolulu, HI 96822, USA, [13]Department of Physics and Astronomy, University of Hawai'i at Mānoa, Honolulu, HI 96822, USA, [14]Department of Physics, The George Washington University, Washington, DC 20052, USA, [15]Heliospheric Physics Laboratory, NASA/GSFC, Greenbelt, MD 20771, USA, [16]Università di Siena and INFN Pisa, I-53100 Siena, Italy, [17]Politecnico di Bari, Department of Mechanics, Mathematics and Management, via Orabona, 4, I-70125 Bari, Italy, [18]Department of Physics, Catholic University of America, Washington, DC 20064, USA, [19]Naval Research Laboratory, Washington, DC 20375, USA

PoS(ICRC2021)590